Neural Computing and Applications (2024) 36:20067–20087
https://doi.org/10.1007/s00521-024-10298-9

ORIGINAL ARTICLE

Breast-NET: a lightweight DCNN model for breast cancer detection and grading using histological samples

Mousumi Saha[1,4] · Mainak Chakraborty[2] · Suchismita Maiti[3] · Deepanwita Das[1]

Received: 6 October 2023 / Accepted: 29 July 2024 / Published online: 10 August 2024

Abstract

Breast cancer is a prevalent and highly lethal cancer affecting women globally. While non-invasive techniques like ultrasound and mammogram are used for diagnosis, histological examination after biopsy is considered the gold standard. However, manual examination of tissues for abnormality is labor-intensive, expensive, and requires prior domain knowledge. Early detection, awareness, and access to specialized medical infrastructure in resource-constrained and remote areas are significant challenges but crucial for saving lives. In recent years, deep learning-based approaches have shown promising results in breast cancer detection, facilitated by advancements in GPU memory, computation power, and the availability of digital data. Motivated by these observations, we propose the Breast-NET deep convolutional neural network model for breast cancer detection and grading using histological images. Our model's performance is evaluated on the BreakHis dataset, and we demonstrate its generalization ability on the Invasive Ductal Carcinoma (IDC) grading and IDC datasets. Extensive experimental and statistical performance analysis, along with an ablation study, validates the efficiency of our proposed model. Furthermore, we demonstrate the effectiveness of transfer learning with seven pre-trained convolutional neural networks for breast cancer detection and grading. Experimental results show that our framework outperforms state-of-the-art approaches in terms of accuracy, space, and computational complexity for the BreakHis, IDC grading, and IDC datasets.

Keywords Deep learning · Breast cancer · Transfer learning · Breast-NET · IDC grading · BreakHis · IDC

1 Introduction

Breast cancer (BC) is the second highest cause of death in women and one of the most serious health issues affecting women worldwide. Female breast cancer has emerged as the leading cancer diagnosis, surpassing lung cancer, with an estimated 2.3 million new cases accounting for 11.7% of all cancer cases [1]. It is followed by lung cancer at 11.4%, colorectal cancer at 10.0%, prostate cancer at 7.3%, and stomach cancer at 5.6% [1]. India is also experiencing a notable increase in breast cancer cases. A study conducted by Globocon in 2020 revealed that every four minutes, a woman in India is diagnosed with breast cancer [2]. The incidence of breast cancer has surpassed cervical cancer, making it the most prevalent cancer among Indian women, with approximately 1,78,000 new cases being diagnosed each year [2]. This concerning rise in breast cancer cases underscores the pressing need for enhanced awareness, early detection, and effective management strategies to

✉ Mousumi Saha
ms.23cs1502@phd.nitdgp.ac.in

Mainak Chakraborty
mainak.chakraborty@mdu.se

Suchismita Maiti
suchismita.maiti@nit.ac.in

Deepanwita Das
deepanwita@cse.nitdgp.ac.in

[1] Department of Computer Science and Engineering, National Institute of Technology, Durgapur, West Bengal 713209, India

[2] School of Innovation, Design and Engineering, Division of Intelligent Future Technologies, Malardalen University, Västerås, Sweden

[3] Department of Information Technology, Narula Institute of Technology, Kolkata, West Bengal 700109, India

[4] Department of Computer Science and Engineering, Narula Institute of Technology, Kolkata, West Bengal 700109, India

mitigate its impact on women's health in India and Globally [2]. Early identification and treatment are now one of the most efficient methods to prevent breast cancer mortality [1]. A physical examination and biopsy, ultrasound, magnetic resonance imaging (MRI), digital mammogram, etc., are typically used to diagnose breast cancer [3]. Biopsy is the only reliable detection method if cancer exists in a suspected location. The method entails collecting and extracting cells or tissue samples for microscopic inspection [3]. Pathologists use visual evaluation of histological samples under a microscope to make the final diagnosis, including grading and staging [3]. However, manual diagnosis is not only laborious and costly, but it also heavily relies on the pathologist's prior knowledge and consistency of pathologic information. Pathologists have a diagnosis accuracy of about 75% percent on average [4]. Thus, computer-aided-diagnostic (CAD) solutions based on the machine learning (ML) framework are being developed to assist physicians during the diagnosis phase and minimize the workload of pathologists and doctors [5]. However, the success of ML models is entirely dependent on manual feature extraction, and the feature extractor employed is subject to human technical expertise [5–8]. As a result of the inadequacy of manual features and the sensitivity of feature extractors, the dependability of ML-based techniques for diagnosing breast cancer is quite poor [5]. Deep learning (DL), on the other hand, has gained popularity recently because to its automatic feature extraction capabilities and is widely utilized to tackle real-world problems such as automated disease diagnosis systems [5–7], human or small unmanned aerial vehicles (SUAVs) activity monitoring [9–14], smart city management [15], etc. Researchers have recently proposed numerous DL-based methods for detecting and classifying breast cancer using histology samples and have shown encouraging results [4, 16–24]. Motivated by the earlier work done by the researchers, in this publication, we have proposed a DL-based framework for detection and determining the stage of breast cancer using histology data. The following are the main findings of this study:

1. We have developed Breast-NET, a lightweight deep learning framework designed for breast cancer detection and grading using histological images.
2. We conducted an ablation study to assess the design considerations for the Breast-NET DCNN model. During this study, we evaluated floating-point operations (FLOPs), the number of parameters, and accuracy while varying the numbers of Breast-NET blocks, attention modules, training with or without early stopping, minority class weight, and the number of layers.
3. We have thoroughly conducted an experimental analysis to exhibit the efficacy of transfer learning in the context of breast cancer detection and grading using histological images.
4. The proposed model and the pre-trained models underwent initial validation and evaluation using the BreaKHis dataset. Additionally, its ability to generalize was demonstrated by assessing its performance on the IDC grading and IDC datasets.

The remainder of this paper is organized as follows: Sect. 2 background, related work, research gaps, and motivation. Section 3 developed novel DCNN architecture and its implementation. Subsequently, the datasets description, ablation study results, experimental results are given in Sect. 4. Section 5 describes the conclusion and future directions.

2 Background and related works

In this section, we will discuss the background research on breast cancer detection and grading using histological images in a summarized manner. The majority of the studies proposed a variety of machine learning and deep learning-based methods for detecting and grading breast cancer, with promising results. Recently, Saini and Susan [16] have presented a transfer learning-based breast cancer detection technique utilizing breast histological images and BreakHis [25] dataset. They have reported that their proposed VGGIN-Net has achieved 96.15% accuracy on the test data. But the proposed approach's computational complexity is huge, thus it's not suitable for field-programmable gate array (FPGA) implementations. Vo et al. [4] have used the stain normalization method as a preprocessing step to reduce the histology image variances. Further, they have adopted data augmentation techniques to increase the number of training samples. In their work inception model was used as a feature extractor. Finally, a gradient-boosting tree was used for classification. They achieved 95.5% (average accuracy of four magnification factors) accuracy on the BreakHis dataset. Preprocessing the histology images includes extra computation power as well as extra processing time and is not suitable for end-to-end training. Toğaçar et al. [26] have proposed a residual and attention mechanism-based CNN model for breast cancer detection using BreakHis dataset. The proposed Breast-Net model achieved 98.8% test accuracy. Misclassification rate of the model is also minimal. Garg et al. [17] have introduced a transfer learning-based ensemble approach for breast cancer detection. They have used MobilNetV2, InceptionV4, and ResNet-50 CNN models as the backbone of their proposed classification network.

They have conducted a detailed experimental analysis using three breast cancer datasets namely, BreakHis, IDC image [22], and BACH [27] datasets. The proposed approach achieved 90.93% (balanced), 92%, and 98.07% accuracy in IDC, BATCH, and BreakHis datasets, respectively. However ensemble learning approaches have limitations like being expensive in terms of space, time, and computational complexity, thus not suitable for real-world applications. George et al. [28] have proposed a transfer learning-based six-stage framework for breast cancer detection using the BreakHis dataset. During the preprocessing stage, the authors used the Macenko stain normalization method on histological images. The nucleus patches are then extracted from the preprocessed samples using a Laplacian of Gaussian filter. The extracted nucleus patches are then fed into the pre-trained CNNs for feature map extraction. Finally, they used 3-norm pooling to fuse the extracted feature maps before passing them to the support vector machine (SVM) classifier. The proposed model achieved good test accuracy of 96.91%, but it requires human intervention during the training and testing phase. George et al. [29] have proposed a nucleus patch-based breast cancer detection technique using BreakHis dataset. They extracted the nucleus patches from the histological images and then fed them to a nine-layer CNN (NucDeep) to extract the patch-level feature map. Further, the extracted patch feature maps from each image are merged into an image-wise single feature map using P -norm pooling. Finally, the SVM classifier is used for binary classification (Benign and Malignant). The proposed model has achieved 96.66% $\pm$ 0.77 accuracy on the BreakHis dataset. Rashmi et al. [18] presented BCHisto-Net CNN for the classification of Benign and Malignant patients using BreakHis and KMC(private) datasets. The proposed model has achieved 95% and 89% accuracy on KMC and BreakHis, respectively. Liu et al. [30] presented a learning binary semantic embedding approach for breast cancer histology image classification utilizing BreakHis dataset. The proposed approach obtained 86% accuracy for the classification task. Gupta and Bhavsar [31] presented a partially independent framework for the classification of Benign and Malignant histological images using the BreakHis dataset. They have reported 94.66% test accuracy (average accuracy of four magnification factors) for binary classification. Pratiher et al. [32] suggested an automated breast cancer classification model based on manifold encoded histological samples using bidirectional long short-term memory (LSTM). The proposed model attained 96.47% accuracy (average accuracy of four magnification factors) for binary classification. Kumar et al. [33] used a VGG-16-based transfer learning approach in conjunction with an SVM classifier to classify H& E-stained histological breast cancer images from the BreakHis dataset. They achieved an average test accuracy of 97% across four magnification factors for binary classification. Gour et al. [34] proposed the ResHist CNN model for breast cancer classification using BreakHis dataset, which was inspired by ResNet-50. The proposed method achieved 84.34% and 92.52% accuracy without and with data augmentation, respectively. Wang et al. [35] created FE-BkCapsNet, a framework based on enhanced routing and feature map fusion for the classification of breast cancer histological samples using the BreakHis dataset. The proposed model classified benign and malignant samples with 93.7% accuracy across different magnification factors. Abbasniya et al. [36] proposed IRv2-CXL, a CAD system that uses transfer learning and ensemble approaches to classify breast cancer histological images. They carried out detailed experiments with sixteen different pre-trained CNNs as feature extractors. On the BreakHis dataset, they reported that the proposed framework achieved 96.46% accuracy. To overcome the class imbalanced problem of the BreakHis dataset, Saini and Susan [37] used deep convolutional generative adversarial network (DCGAN) to generate synthetic images for the minority class (Benign). Furthermore, the balanced dataset was used to train a pre-trained VGG-16 CNN model, which scored 94.75% on the final classification task. Man et al. [38] proposed a three-stage framework, DenseNet121-AnoGAN, for histological breast cancer image classification. They used AnoGAN to screen mislabeled patches and DenseNet for classification. Over the four magnifying factors, the proposed approach achieved an average overall test accuracy of 91.77%.

Sharma and Mehra [39] utilized the AlexNet pre-trained model for multi-class classification of breast histological images using the BreakHis dataset. They found that fine-tuning a deep or shallow network to a moderate level is the best solution for magnification-dependent histological sample classification. They achieved 85.83% test accuracy (average accuracy of four magnification factors) for eight class classifications. However, the proposed model suffers from false-positive results. Similarly, Bardou et al. [40] employed the CNN model for binary and multi-class classification of breast cancer histological images using the BreakHis dataset. The proposed approach is based on handcrafted feature extraction from the histology images and utilization of handcrafted feature maps for binary and multi-class classification using traditional machine learning techniques and deep learning techniques. They have shown that the performance of deep learning is far better compared to machine learning. They achieved 97.36% test accuracy for binary classification and 85.04% test accuracy for eight class classifications (average accuracy of four magnification factors).

Dimitropoulos et al. [41] proposed a Grassmannian VLAD encoding method for classifying benign and

malignant classes using the BreakHis dataset, as well as Grading Invasive Breast Carcinoma (GIBC) by creating a dataset containing 300 annotated histological images ranging from grade 1 to grade 3. They have reported that the proposed method achieved 91.38% and 95.8% accuracy on BreakHis and their own dataset. The proposed model performance depends on the precise extraction of image patches. They reported that the (8X8) patches of the original images provided the best classification results, but we know that small patch-based approaches are insensitive to nonlocal texture features. Li et al. [42] proposed a multi-task DCNN model for automatic grading microscopy invasive breast carcinoma images using the dataset mentioned in [41] and classification of breast cancer using BreakHis dataset. They have used the Xception network pre-trained on the ImageNet dataset as a backbone of their proposed model. They have reported 93.43% and 93.01% test accuracy on BreakHis and GIBC dataset, respectively. Another work by Nanni et al. [19] presented a three-stage approach (feature extraction + dimensionality reduction + SVM classifier) for breast cancer grading using the GIBC dataset. On the GIBC dataset, the experimental results show that ReNet50 as a feature extractor combination with global entropy pooling and SVM classifier provides 93.7% accuracy, and GoogleNet as a feature extractor combination with global entropy pooling and SVM classifier provides 93.7% accuracy. Yan et al. [43] proposed a two-stage network namely NGNet for grading microscopy invasive breast carcinoma images. In stage one, they extracted the nucleus region from each pathology sample. In stage two the original images along with the corresponding nucleus regions are passed to the NGNet for final prediction results. The proposed approach achieved 93.4% test accuracy. Yan et al. [20] designed nuclei aware convolutional network for breast cancer grading using histological images. The model was trained using the GIBC dataset. They have reported 92.2% accuracy in grading invasive ductal carcinoma (IDC). Lagree et al. [44] presented a computer-aided diagnosis (CAD) system for grading breast cancer using machine learning techniques. They also demonstrated that pathology imaging biomarkers can be used to improve the performance of the CAD system. The proposed CAD system was trained and tested using the GIBC dataset, and it achieved 78.57% test accuracy using the ensemble approach (logistic regression and random forest classifier). Abdelli et al. [21] used a transfer learning technique for grading breast cancer histological images. As the network's backbone, they used the ResNet-50 and MobileNet CNN models. The proposed model was trained on the GIBC dataset. They achieved 92.39% and 93.48% test accuracy for ResNet-50 and MobileNet, respectively.

Cruz-Roa et al. [22], on the other hand, presented Invasive Ductal Carcinoma (IDC) datasets with 277,524 non-IDC and IDC histological patches of 50x50 dimensions. The dataset was experimentally validated by training a three-layered CNN model, and classification performance was thoroughly compared with standard handmade feature techniques. The proposed model attained a test accuracy of 84.23%. Liu et al. [5] suggested an AlexNet-based transfer learning strategy for detecting breast cancer utilizing the BreakHis and Invasive Ductal Carcinoma (IDC) [22] datasets. In addition, to avoid overfitting during the learning process, they introduced a novel low-entropy output penalty in softmax cross-entropy learning. The proposed method achieved 98% average accuracy across four distinct magnifying factors for the BreakHis dataset and 86.31% for the IDC dataset. Celik et al. [23] used pre-trained DCNN architecture to classify IDC breast cancer histology samples. They reported 90.96% test accuracy utilizing a ResNet-50-based transfer learning technique. Wang et al. [45] presented a hybrid DCNN framework based on CNN-GRU for IDC classification using IDC datasets. The proposed system achieved an accuracy of 86.21%. Romero et al. [46] utilized the Inception CNN model for the classification of IDC and non-IDC samples and achieved 89% test accuracy. In [24], Reza and Ma used the IDC and BreakHis datasets to automatically classify breast cancer samples using a six-layer CNN framework. The proposed method achieved test accuracy of 85.48% and 85.62% for the IDC and BreakHis datasets, respectively. To solve the imbalance dataset problem, the authors proposed an oversampling method, although we know that oversampling is particularly prone to overfitting. Janowczyk and Madabhushi [47] adopted an AlexNet-based transfer learning framework to classify IDC histological patches and attained 84.68% test accuracy. Abdolahi et al. [48] created a four-convolution-layered CNN model for detecting IDC and non-IDC breast cancer samples. They achieved an accuracy of 85.62% on the IDC [22] dataset.

2.1 Research gaps and motivation

Breast cancer detection using histological images has shown promising results with deep learning techniques, but there are still some research gaps that present opportunities for further improvement. Many earlier approaches proposed new or utilized pre-trained deep learning models, such as convolutional neural networks. However, some of these methods heavily rely on manual feature extraction and multiple preprocessing stages, including nucleus separation, stain normalization, and segmentation, which can significantly impact the final classification outcome. The accuracy of these techniques is highly dependent on the quality of segmentation and feature extraction from manually specified regions. Manual annotation of nuclei in histology images is laborious and time-consuming, and

manual feature extraction may not adequately capture intricate and nonlinear relationships in the data. In contrast, automated feature learning techniques, such as deep learning, have the potential to discover complex patterns and representations that manual approaches may miss. As datasets grow in size and complexity, hand-crafting features becomes increasingly challenging and time-consuming. Moreover, stain normalization approaches may unintentionally omit or distort essential diagnostic information present in the original images, and there is a lack of standard metrics for evaluating the performance of stain normalization methods. Additionally, some research employed transfer learning-based techniques for diagnosing breast cancer. However, one significant drawback is that the pre-trained models used for transfer learning might not properly represent the specific characteristics of the breast cancer datasets, leading to suboptimal performance. Furthermore, end-to-end training and FPGA implementation of these methods are not always feasible. To address these limitations, we propose a lightweight end-to-end trainable deep convolutional neural network (DCNN) model for automatic breast cancer detection and grading using histological images in this study. The development of such a model holds promise for improving breast cancer diagnosis, especially in resource-constrained settings and remote areas with limited access to specialized healthcare facilities.

3 Proposed method

In this section, we present the architecture and implementation details of the proposed Breast-NET DCNN model for breast cancer detection and grading using histological images.[1]

3.1 Breast-NET architecture

We have proposed a lightweight DCNN model called Breast-NET to detect breast cancer and grade it using histology images. The primary goal of this design consideration is to create a compact model appropriate for field-programmable gate array (FPGA) device implementation. The proposed model's block diagram and summary are presented in Fig. 1 and Table 1. (The model summary in Table 1 is based on the BreakHis and IDC grading datasets.)

The input shape for the IDC dataset is 50x50x3, and the output shape will also be modified accordingly. The Breast-NET DCNN model has 52 layers, which are as follows: 16 separable convolutional layers, 13 batch normalization layers, 6 add layers, 6 activation layers, 4 global average pooling layers, 3 reshape layers, 1 max-pool layer, 1 softmax layer, 1 dropout layer, and 1 input layer. The histopathological images are initially resized to 256x256x3 for BreakHis and IDC grading dataset and 50x50x3 for IDC dataset, normalized with a 1./255 rescaling factor, and then real-time augmented with 0.05 shear intensity, 0.05 zoom range, 20^o rotation range, 0.1 width & height shifting range, randomly flip inputs vertically & horizontally, and nearest fill mode, using ImageDataGenerator from the Keras library during the preprocessing phase. The preprocessed histology samples are then passed to the first convolution layer having 64 filters of dimension (3×3) with stride 2. In order to reduce the floating-point operations (FLOPs) of the proposed model, we have used separable convolutional layers instead of traditional convolutional layers. The output feature map of shape (128,128,64) is then passed to a (3×3) max-pool layer with stride 2 followed by a batch normalization layer. The max-pool layer downscales the output feature map and aids in extracting the most relevant feature from the output feature map of the initial convolutional layer. The inclusion of this layer at the start also aids in reducing computing complexity. After most of the convolutional layers, we employed a batch normalization layer to accelerate the training process and normalize the output feature map coming out from the convolutional layers. The output feature map of dimension $F_M \in \mathbb{R}^{H\times W\times D}$ is then passed to the first Breast-NET module. The proposed Breast-NET architecture consists of three consecutive Breast-NET modules as shown in Fig. 1. Each Breast-NET module consists of three concurrent routes that use grouped convolutions with three different dimension filters on the same input tensor. This facilitates the extraction of multilevel feature representations from input feature maps. Path one involves passing the output feature maps from the max-pooling or activation layer of dimension $F_X \in \mathbb{R}^{H_i\times W_i\times D_i}$ to a convolutional layer with $D_i^{MOD_i}$ 1×1 filters and stride 1. The number of filters ($D_i^{MOD_i}$) in the three Breast-NET modules is 64, 96, and 120, as shown in Table 1. The output tensor of the 1×1 convolutional layer is then transferred to a batch normalization layer, which produces an output feature map of dimension $F_{B_i}^{MOD_i} \in \mathbb{R}^{H_i^{MOD_i}\times W_i^{MOD_i}\times D_i^{MOD_i}}$. The path one of Breast-NET modules is presented by (1).

$$F_{P1}^{MOD_i}(x) = F_{B_i}^{MOD_i}(\sigma(F_{C_i}^{MOD_i}(F_X * w_i + b_i))) \quad (1)$$

where $F_{B_i}^{MOD_i}$ and $F_{C_i}^{MOD_i}$ are the i^{th} batch normalization and convolutional layer of path one of the i^{th} module, respectively. σ, F_X, w_i and b_i represent ReLU activation, output feature maps of the max-pooling or activation layer,

[1] Source code is available at https://github.com/mainak15/Breast-NET.

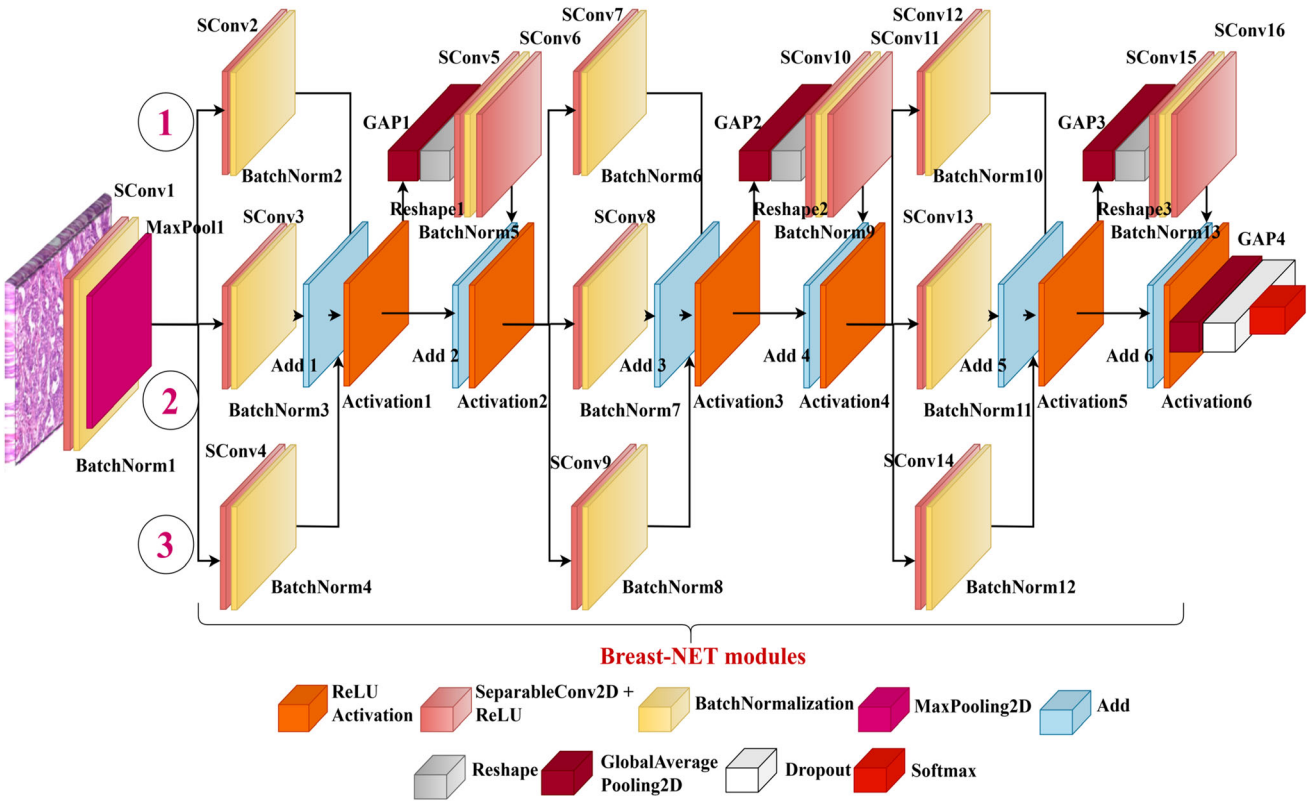

Fig. 1 The block diagram of the proposed Breast-NET DCNN model

weights and bias, respectively. Similarly, in paths two and three, we used 3×3 and 5×5 size filters in the convolutional layer to extract multilevel feature maps. The path two and three can be expressed by the following (2) and (3), respectively.

$$F_{P2}^{MOD_i}(x) = F_{B_{i+1}}^{MOD_i}(\sigma(F_{C_{i+1}}^{MOD_i}(F_X * w_i + b_i))) \tag{2}$$

$$F_{P3}^{MOD_i}(x) = F_{B_{i+2}}^{MOD_i}(\sigma(F_{C_{i+2}}^{MOD_i}(F_X * w_i + b_i))) \tag{3}$$

where $F_{B_{i+1}}^{MOD_i}$, $F_{B_{i+2}}^{MOD_i}$, and $F_{C_{i+1}}^{MOD_i}$, $F_{C_{i+2}}^{MOD_i}$ represent the batch normalization and convolutional layer of paths two and three, respectively. In order to extract multilevel feature representations from the input, we used 1×1, 3×3, and 5×5 size filters, as well as stride one and the same padding settings, in each Breast-NET module. Finally, in the addition layer, the batch normalization layers output feature map of dimension $F_{P1}^{MOD_i}, F_{P2}^{MOD_i}, F_{P3}^{MOD_i} \in \mathbb{R}^{H_i^{MOD_i} \times W_i^{MOD_i} \times D_i^{MOD_i}}$ of the three paths is element-wise added using (4).

$$F_{Add_i}^{MOD_i}(x) = F_{P1}^{MOD_i}(x) \oplus F_{P2}^{MOD_i}(x) \oplus F_{P3}^{MOD_i}(x) \tag{4}$$

The output $F_{Add_i}^{MOD_i}$ of the addition layer is then activated by a ReLU activation layer using (5).

$$F_{Act_i}^{MOD_i}(x) = \sigma(F_{Add_i}^{MOD_i}(x)) \tag{5}$$

where, σ is the ReLU activation. The activation layer's output feature map is then sent to a channel attention module (CAM) in each Breast-NET module. The key reason for including a CAM module in the Breast-NET architecture is to force CNN to learn and focus on critical hallmark signatures rather than irrelevant background information. The CAM module consists of one global average pooling (GAP), one reshape, two 1×1 separable convolutions, one addition, one activation and one batch normalization layer. The CAM module takes an input feature map of dimension $F_{Act_i}^{MOD_i} \in \mathbb{R}^{H_i^{MOD_i} \times W_i^{MOD_i} \times D_i^{MOD_i}}$, apply average pooling on the height and width dimensionality for all the channels by GAP layer, and then the resulting 2D tensor $(batch_d im, D_i^{MOD_i})$ to a reshape layer, which project back the tensor to dimension $(1 \times 1 \times D_i^{MOD_i})$. Finally, the reshape layer's output feature map of dimension $F_{RE_i}^{MOD_i} \in \mathbb{R}^{1 \times 1 \times D_i^{MOD_i}}$ is given to a $F_{C_{i+4}}^{MOD_i}$ convolution layer, followed by batch normalization $F_{B_{i+3}}^{MOD_i}$ and a $F_{C_{i+3}}^{MOD_i}$ convolution layer, which is element-wise merged with the input feature map $F_{Act_i}^{MOD_i} \in$

Table 1 Breast-NET DCNN model's summary

Layer (type)	Output shape	Param #	Layer (type)	Output shape	Param #	Layer (type)	Output shape	Param #
InputLayer	(None, 256, 256, 3)	0	Activation2	(None, 43, 43, 64)	0	SConv14 5×5/1	(None, 43, 43, 120)	14040
SConv1 3×3/2	(None, 128, 128, 64)	283	SConv7 1×1/1	(None, 43, 43, 96)	6304	BatchNorm10	(None, 43, 43, 120)	480
BatchNorm1	(None, 128, 128, 64)	256	SConv8 3×3/1	(None, 43, 43, 96)	6816	BatchNorm11	(None, 43, 43, 120)	480
MaxPool1 3×3	(None, 43, 43, 64)	0	SConv9 5×5/1	(None, 43, 43, 96)	7840	BatchNorm12	(None, 43, 43, 120)	480
SConv2 1×1/1	(None, 43, 43, 64)	4224	BatchNorm6	(None, 43, 43, 96)	384	Add5	(None, 43, 43, 120)	0
SConv3 3×3/1	(None, 43, 43, 64)	4736	BatchNorm7	(None, 43, 43, 96)	384	Activation5	(None, 43, 43, 120)	0
SConv4 5×5/1	(None, 43, 43, 64)	5760	BatchNorm8	(None, 43, 43, 96)	384	GAP3	(None, 120)	0
BatchNorm2	(None, 43, 43, 64)	256	Add3	(None, 43, 43, 96)	0	Reshape3	(None, 1, 1, 120)	0
BatchNorm3	(None, 43, 43, 64)	256	Activation3	(None, 43, 43, 96)	0	SConv15 1×1/1	(None, 1, 1, 120)	14640
BatchNorm4	(None, 43, 43, 64)	256	GAP2	(None, 96)	0	BatchNorm13	(None, 1, 1, 120)	480
Add1	(None, 43, 43, 64)	0	Reshape2	(None, 1, 1, 96)	0	SConv16 1×1/1	(None, 1, 1, 120)	14640
Activation1	(None, 43, 43, 64)	0	SConv10 1×1/1	(None, 1, 1, 96)	9408	Add6	(None, 43, 43, 120)	0
GAP1	(None, 64)	0	BatchNorm9	(None, 1, 1, 96)	384	Activation6	(None, 43, 43, 120)	0
Reshape1	(None, 1, 1, 64)	0	SConv11 1×1/1	(None, 1, 1, 96)	9408	GAP4	(None, 120)	0
SConv5 1×1/1	(None, 1, 1, 64)	4224	Add4	(None, 43, 43, 96)	0	Dropout	(None, 120)	0
BatchNorm5	(None, 1, 1, 64)	256	Activation4	(None, 43, 43, 96)	0	Softmax	(None, 8)	968
SConv6 1×1/1	(None, 1, 1, 64)	4224	SConv12 1×1/1	(None, 43, 43, 120)	11736	Total params: 136,491		
Add2	(None, 43, 43, 64)	0	SConv13 3×3/1	(None, 43, 43, 120)	12504	Trainable params: 134,123		

$\mathbb{R}^{H_i^{MOD_i} \times W_i^{MOD_i} \times D_i^{MOD_i}}$ in the addition layer ($F_{Add_{i+1}}^{MOD_i}$) and activated by the ReLU activation layer ($F_{Act_{i+1}}^{MOD_i}$) using (6).

$$F_{Act_{i+1}}^{MOD_i}(x) = \sigma[\sigma(F_{C_{i+4}}^{MOD_i}(F_{B_{i+3}}^{MOD_i}(\sigma(F_{C_{i+3}}^{MOD_i}(F_{RE_i}^{MOD_i}(F_{GAP_i}^{MOD_i}(F_{Act_i}^{MOD_i})) * w_{i+3} + b_{i+3}))) * w_{i+4} + b_{i+4})) \oplus F_{Act_i}^{MOD_i}(x)] \tag{6}$$

Following that, we passed the output feature map of the first Breast-NET module to the other two sequential Breast-NET modules, as shown in Eq.(7) and in Fig. 1.

$$F_{Act_{i+1}}^{MOD_{i+2}}(x) = F_{Act_{i+1}}^{MOD_{i+2}}(F_{Act_{i+1}}^{MOD_{i+1}}(F_{Act_{i+1}}^{MOD_i}(x))) \tag{7}$$

After that, we send the third Breast-NET module's output feature map $F_{Act_{i+1}}^{MOD_{i+2}}(x)$ to a GAP layer ($F_{GAP_{i+3}}$) and a dropout layer (F_{DROP}). The output tensor is then sent to the classification layer, which classifies the histopathology images. The classification layer is made up of eight/three neurons for multi-class classification and two neurons for binary classification, all of which are activated by the softmax activation function. The total number of parameters in our DCNN model is only 136,491, demonstrating the lightweight nature of the Breast-Net architecture.

3.2 Implementation details

The proposed Breast-NET architecture was implemented, and the experiments were carried out using a machine

equipped with NVIDIA-SMI 462.62, Driver Version 462.62, CUDA Version: 11.3, cuDNN 8.2.1, GeForce GTX 1650 4096MiB, Python 3.9.12, tensorflow-gpu 2.6.0, keras-gpu 2.6.0, matplotlib 3.5.2, and scikit-learn 1.1.1. The proposed model's hyper-parameters are tuned and optimized using trial and error methods, and the number of Breast-NET modules, filter size, the inclusion of the channel attention, and whether or not class weight should be given has been decided based on the ablation study; this is discussed in detail in the experimental results performance analysis section. We employed a Glorot uniform kernel initializer and constant bias initializer (value = 0.2) in all convolution layers to enable efficient training and convergence of the DCNN model. The number of filters utilized, their dimension, and the stride values of each layer are all listed in Table 1. We have end-to-end trained the DCNN model up to 300 epochs while experimenting with the BreakHis and IDC grading datasets, but in the case of the IDC dataset, we used early stopping by monitoring the validation losses (if the validation loss fails to decrease in the next ten epochs) during training, as we observed that training up to 300 epochs causes the model to overfit. We gave minority classes more weightage during the training phase of the BreakHis dataset because it has a high degree of imbalance, making it difficult to achieve good classification accuracy; but we did not do so for the IDC grading and IDC dataset because they are balanced datasets. The batch size was set to eight during the training phase, and the model was optimized using the Adam optimizer with a learning rate $1e^{-4}$. We used the categorical cross-entropy loss function to minimize the difference between the ground truth and the prediction while adjusting the weight and bias during training. In our experiments with transfer learning-based pre-trained CNNs, we employed the same training strategy as our proposed Breast-NET DCNN model, which includes using the same optimizer, learning rate, and batch size to ensure a fair comparison. Additionally, we utilized early stopping to avoid overfitting while experimenting with transfer learning-based approaches for all datasets.

4 Experimental results and performance analysis

4.1 Dataset

The proposed Breast-NET DCNN architecture is validated and evaluated utilizing three breast histopathology image datasets with varied hallmark signature characteristics. The first dataset we have used for performance investigation of the proposed DCNN model is BreakHis [25] dataset. BreakHis is one of the largest open source datasets, featuring 7909 histology samples with magnification factors of 400, 200, 100, and 40. The collection includes benign and malignant breast cancer histology images. Each kind of breast cancer is further subdivided into four subgroups. The benign class includes tubular adenoma, phyllodes tumor, fibroadenoma, and adenosis, while the malignant class include papillary carcinoma, mucinous carcinoma, lobular carcinoma, and ductal carcinoma (sample histopathology images are shown in Fig. 2). The second dataset we have used for IDC grading was released by Dimitropoulos et al. [41]. The dataset consists of 300 histological samples altogether, divided into three grades (Grade 3: 91, Grade 2: 102, and Grade 1: 107 samples), each with a 1280 × 960 resolution and representing 21 distinct patients. (Figure 3 displays a few examples of histopathological images.) The Breast-NET DCNN architecture is further evaluated on publicly available IDC dataset released by Cruz-Roa et al. [22]. The dataset comprises 277,524 histological patches of 50x50 dimensions, of which 78,786 fall under the IDC positive category and 198,738 the IDC negative category. (Sample histopathology images are shown in Fig. 4.) In the case of BreakHis and IDC datasets, we randomly divided the dataset in an 80:10:10 ratio for train, test, and validation; for IDC grading datasets, the split was 70:15:15.

4.2 Ablation study results

We have conducted a detailed ablation study to demonstrate the design considerations for the Breast-NET architecture, and the results are displayed in Table 2. For this ablation study, we calculated the FLOPs, number of parameters, and accuracy using different numbers of Breast-NET blocks, attention modules, training with or without early stopping, minority class weight, and number of layers. We examined the trade-off between the number of layers, total number of model parameters, FLOPs, and classification accuracy when settling on the final configuration. We can see that increasing the number of Breast-NET blocks does not improve testing accuracy, but rather increases computing complexity. Table 2 shows that up to three consecutive Breast-NET blocks, accuracy increases to 98% with FLOPs of 0.141G, but as we add more Breast-NET blocks to the architecture, accuracy decreases while FLOPs increase. For example, the DCNN model with six consecutive Breast-NET blocks achieved 95% accuracy with FLOPs of 0.821G. Similarly, if we did not include the channel attention within the three Breast-NET blocks, but instead reduced the learning rate and used early stopping, the model only achieved 94% accuracy with FLOPs 0.07G. On the other hand, if we do not employ early stopping, but instead cut the learning rate due to no improvement in the validation loss and include channel attention during

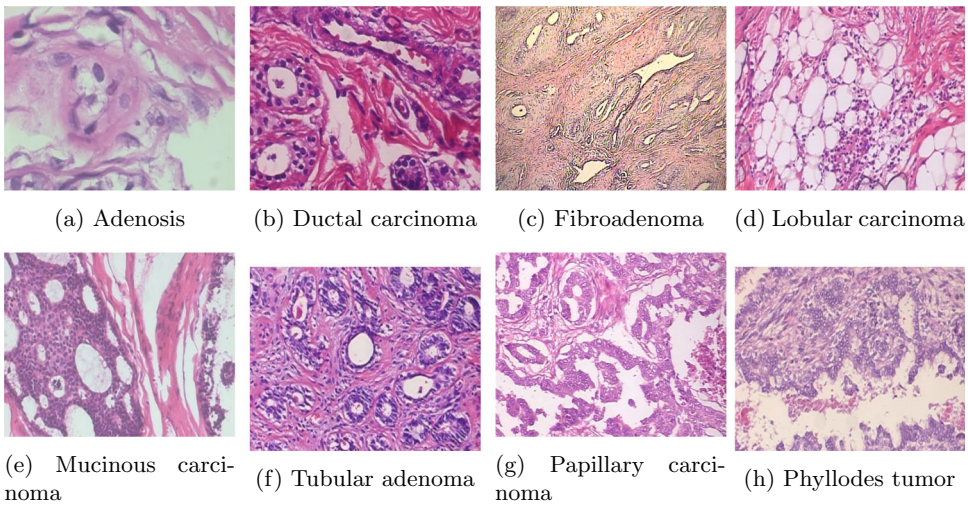

(a) Adenosis (b) Ductal carcinoma (c) Fibroadenoma (d) Lobular carcinoma

(e) Mucinous carcinoma (f) Tubular adenoma (g) Papillary carcinoma (h) Phyllodes tumor

Fig. 2 Examples of histopathological images taken from BreakHis dataset [25]

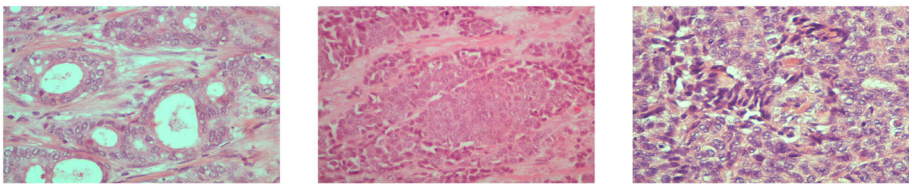

(a) Grade 1 (b) Grade 2 (c) Grade 3

Fig. 3 Examples of histopathological images taken from IDC grading dataset [41]

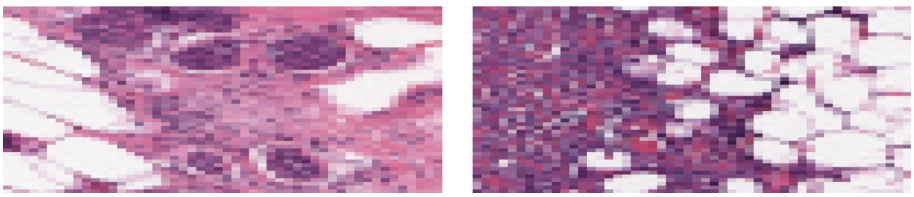

(a) IDC negative (b) IDC positive

Fig. 4 Examples of histopathological images taken from IDC dataset [22]

training, the model achieves 97.22% accuracy with FLOPs of 0.141G. Thus, we included channel attention within the three Breast-NET blocks, weighted minority classes in the case of an imbalance dataset, trained the model end-to-end for 300 epochs, and used a fixed learning rate as a final setup in our proposed model, we achieved 98%, FLOPs of 0.141G, and 0.13M total trainable parameters.

4.3 Results on the BreakHis dataset

We have conducted detailed experimental analysis and computed statistical performance analysis metrics such as classification report, receiver operating characteristics (ROC) curves, confusion matrix, misclassification rate, and FLOPs to demonstrate the efficiency of the Breast-NET architecture in the BreakHis dataset for binary or eight-class classification. Figure 5 depicts the ROC curves for binary and multi-class classification. The area under the curve values in both curves are either equal to or greater than 99% and are not overlapped, demonstrating the superiority of the DCNN models to separate the key feature information available in eight types of cancer patients' histological samples. The accuracy and loss plots for binary and eight-class classification are shown in Fig. 6. It is evident from both plots that the training and validation loss curves converge to a low value, which indicates a good fit for both classification tasks. The confusion matrix of the models for binary and eight-class classification is shown in Fig. 7. We can see that the models' misclassification error is just 0.0189 and 0.0966 for binary and multi-class classification, respectively, indicating that false-positive and false-negative rates for breast cancer classification are low. Similarly, the classification reports for the Breast-NET model are highlighted in Tables 3 and 4. We can notice that the model attained 98.11% testing accuracy, 97% precision, 98% recall, and 98% F1-score for binary classification and 90.34% testing accuracy, 86% precision, 92% recall, and 89% F1-score for multi-class classification.

Table 2 Ablation study of the Breast-NET model

No of Breast-NET blocks	Layers	# Params (M)	FLOPs	Accuracy (%)
1 Breast-NET block (with early stopping, with learning rate reduction, with class weight, and with channel attention module)	22	0.03	0.039G	93.48
2 Breast-NET block (with early stopping, with learning rate reduction, with class weight, and with channel attention module)	37	0.06	0.070G	94
4 Breast-NET block (with early stopping, with learning rate reduction, with class weight, and with channel attention module)	67	0.25	0.256G	96
5 Breast-NET block (with early stopping, with learning rate reduction, with class weight, and with channel attention module)	82	0.47	0.466G	95
6 Breast-NET block (with early stopping, with learning rate reduction, with class weight, and with channel attention module)	97	0.78	0.821G	95
3 Breast-NET block (with early stopping, with learning rate reduction, with class weight, and without channel attention module)	31	0.13	0.07G	94
3 Breast-NET block (without early stopping, with learning rate reduction, with class weight, and with channel attention module)	52	0.13	0.141G	97.22
3 Breast-NET block (without early stopping, without learning rate reduction, with class weight, and with channel attention module)	52	0.13	0.141G	98.11

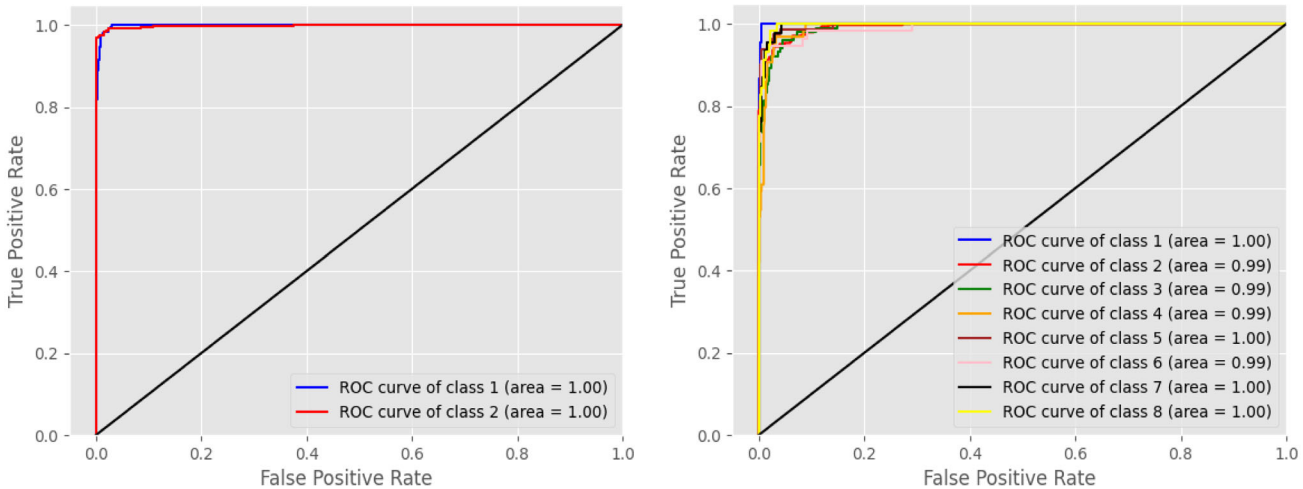

(a) Binary classification (b) Eight-class classification

Fig. 5 The ROC curves of the Breast-NET model using the BreakHis dataset

In addition, we assessed the performance of existing transfer learning-based pre-trained CNN models on the BreakHis dataset for both multi-class and binary classification. Table 5 compares the proposed model's performance against well-known pre-trained CNNs in terms of the number of layers, disk space for weight files in MB, number of model parameters, FLOPs, and accuracy. We can observe that the computational complexity of DenseNet-201, Inception-v3, VGG-16, VGG-19, and ResNet-50 in terms of FLOPs is too high, rendering them inappropriate for FPGA implementation. MobileNet V1 and V2 complexity are minimal, making them appropriate for FPGA implementation, however, the multi-class and binary classification accuracy is only 89.54%, 80% and 97.42%, 93.94%, respectively.

Furthermore, we have conducted statistical comparisons of the Breast-NET model with state-of-the-art models on the BreakHis dataset for binary-class and multi-class classification, as shown in Table 6. We analyzed six factors for this comparison: classification type, methods/models utilized, precision, recall, F1-score, and accuracy. In order to compare the model's performance fairly, we have taken into account their average accuracy, precision, recall, and f1 score for four different magnification factors. In the case

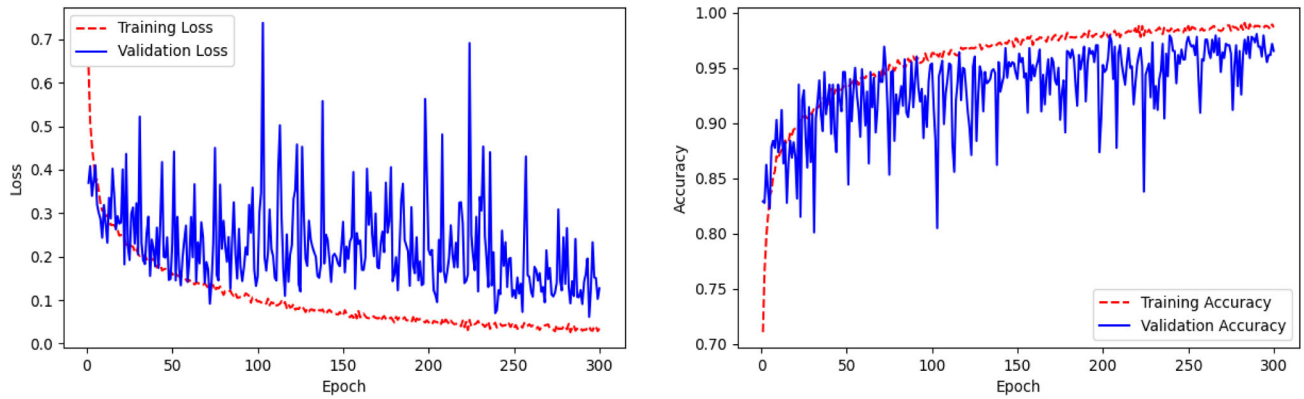

(a) Binary classification

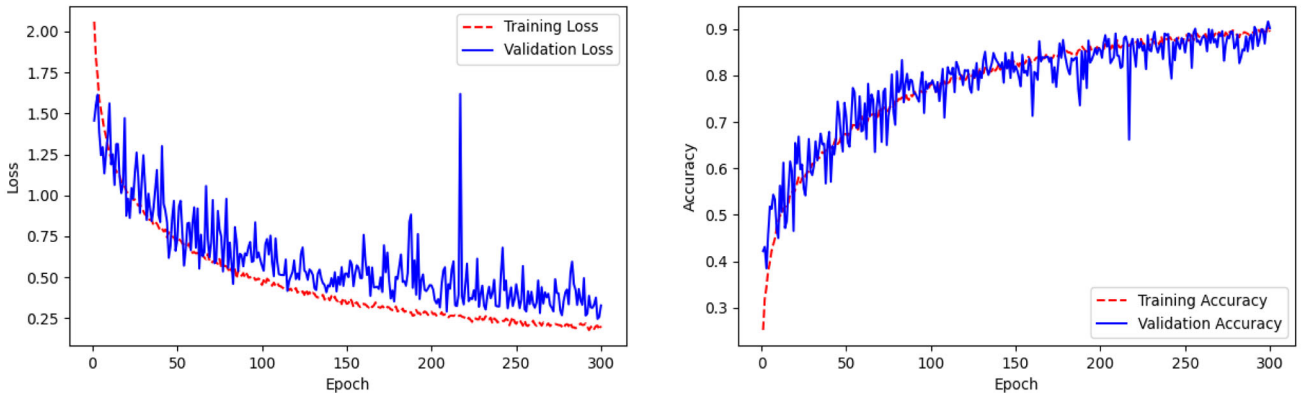

(b) Eight-class classification

Fig. 6 The loss and accuracy plots of the Breast-NET model using the BreakHis dataset

of malignant and benign classification, Saini and Susan [16] employed VGGIN-Net and reached 96.15% accuracy with an F1-score of 0.91/0.75, however, their model suffers from false-positive and false-negative outcomes. Vo et al. [4] used transfer learning-based Inception CNN together with gradient-boosting tree as a classifier and achieved only 95% test accuracy. Toaçar et al. [26] suggested the BreasNet model and achieved 98.8% classification accuracy, their model performance is pretty close to ours, but the proposed model computational cost (FLOPs: 3.7G) is 26 times that of our DCNN model. Similarly, Garg et al. [17] conducted experiments with MobilNetV2, InceptionV4, and ResNet-50 pre-trained CNNs-based Ensemble approach, but ensemble learning suffers from issues such as overfitting and underfitting, end-to-end training is time-consuming and primarily computationally expensive. George et al. [28] used a transfer learning-based six-stage framework for breast cancer classification and achieved 96.91% test accuracy, but the suggested approach required manual feature extraction, making end-to-end training and on-device deployment impossible. Rashmi et al. [18] suggested BCHisto-Net CNN for Malignant & Benign patient histology sample classification, and achieved 89% classification accuracy; however, the proposed model has a too high misclassification rate. Liu et al. [30] suggested a binary semantic embedding approach for breast cancer diagnosis. The proposed technique reached 86% accuracy, although the misclassification rate is also high, as Rashmi et al. [18]. Gupta and Bhavsar [31] developed a partially independent framework for breast cancer screening and achieved 94.66% test accuracy. Pratiher et al. [32] proposed a manifold encoding and bidirectional LSTM-based framework and achieved 96.47% classification accuracy, although the suggested model required human involvement during the preprocessing stage. Kumar et al. [33] used pre-trained VGG-16 and SVM classifiers for H& E-stained malignant & benign sample classification and reached 97% accuracy; however, due to the large computational overhead, the suggested model is not suited for FPGA implementations. Gour et al. [34] proposed ResHist CNN for breast cancer diagnosis and achieved 92.52% accuracy. They used a manual data augmentation strategy to increase the number of samples in the minority class, hence the models' performance must be tested with raw histology

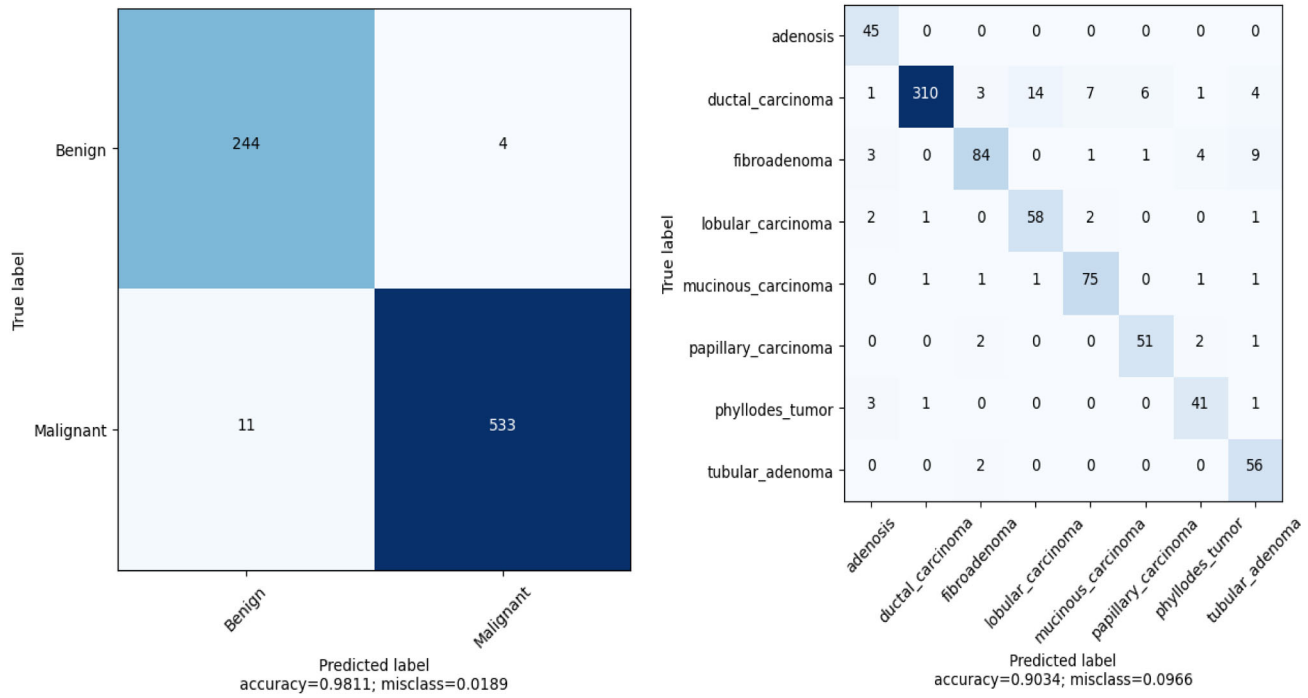

(a) Binary classification (b) Eight-class classification

Fig. 7 The confusion matrix of the Breast-NET model using the BreakHis dataset

Table 3 Classification report of Breast-NET model on the BreakHis dataset for binary classification

	Precision	Recall	F1-score
Class Benign	0.96	0.98	0.97
Class Malignant	0.99	0.98	0.99
Accuracy			98.11
Macro avg	0.97	0.98	0.98
Weighted avg	0.98	0.98	0.98

Table 4 Classification report of Breast-NET model on the BreakHis dataset for multi-class classification

	Precision	Recall	F1-score
Class adenosis	0.83	1.00	0.91
Class ductal carcinoma	0.99	0.90	0.94
Class fibroadenoma	0.91	0.82	0.87
Class lobular carcinoma	0.79	0.91	0.85
Class mucinous carcinoma	0.88	0.94	0.91
Class papillary carcinoma	0.88	0.91	0.89
Class phyllodes tumor	0.84	0.89	0.86
Class tubular adenoma	0.77	0.97	0.85
Accuracy			90.34
Macro avg	0.86	0.92	0.89
Weighted avg	0.91	0.90	0.90

samples. Wang et al. [35] and Abbasniya et al. [36] proposed the FE-BkCapsNet and IRv2-CXL frameworks for breast cancer diagnosis and achieved 93.7% and 96.46% test accuracy, respectively, but both models suffer from high false-positive and false-negative findings. Saini and Susan [37] used a pre-trained VGG-16 DCNN model and achieved 94.75% accuracy in Malignant and Benign classification. To increase the number of samples in the minority class, they constructed synthetic images using DCGAN, hence the correlation of these artificially generated images with the raw histology samples must be investigated. Man et al. [38] used the DenseNet121-AnoGAN architecture for breast cancer diagnosis and achieved 91.77% test accuracy, although the proposed model has high computational costs. Heikal et al. [55] proposed a custom CNN model for classifying benign and malignant breast tumors using the BreakHis dataset, reporting that their model outperformed existing pre-trained CNNs like ResNet-50V2, VGG-16, EfficientNetB0, and MobileNetV3, achieving 93.13% accuracy for binary classification. Rana et al. [56] employed a transfer learning-based approach with seven pre-trained CNNs for binary classification of breast tumors using the BreakHis dataset, finding that Xception achieved the highest accuracy at 83.09%.

Table 5 Comparison of the Breast-NET model performance with other popular transfer learning-based pre-trained DCNN models on the BreakHis dataset for binary-class, and multi-class classification

DCNNs	Input dimension	Layers	Size (Mb)	# Params (M)	FLOPs	Accuracy for binary-class	Accuracy for multi-class
MobileNetV2 [49]	$224 \times 224 \times 3$	157	23.4	2.2	0.30G	93.94%	80%
VGG-19 [50]	$224 \times 224 \times 3$	24	166	20	19.6G	69%	63%
ResNet-50 [51]	$224 \times 224 \times 3$	178	124	23.5	3.88G	77%	71%
VGG-16 [50]	$224 \times 224 \times 3$	21	155	14.7	15.5G	97%	65%
MobileNetV1 [52]	$224 \times 224 \times 3$	89	37.1	3.2	0.57G	97.42%	89.54%
Inception-v3 [53]	$299 \times 299 \times 3$	314	192	21.8	5.73G	95.08%	83%
DenseNet-201 [54]	$224 \times 224 \times 3$	709	124	28.3	4.32G	97.12%	89%
Breast-NET	$256 \times 256 \times 3$	52	1.86	0.136	0.141G	98.11%	90.34%

Ijaz et al. [57] introduced a convolutional block attention module-based VGGNet for classifying H &E-stained breast histopathology images, with their CBAM-VGGNet model attaining an average accuracy of 97.66% across all magnification factors on the BreakHis dataset. Maleki et al. [58] employed a pre-trained DenseNet-201 model combined with an XGBoost classifier for binary classification on the BreakHis dataset, achieving a test accuracy of 91.9%. On the other hand, Bardou et al. [40] employed CNN models and standard ML techniques for binary and multi-class classification and achieved 97.36% and 85.04% accuracy, respectively. The efficacy of the suggested approaches is entirely dependent on handcrafted feature extraction, therefore end-to-end training or on-device implementation is not viable; also, the model suffers from false-positive and false-negative outcomes. Finally, the results of our studies show that the current strategy outperforms the others in both binary and multi-class classifications.

4.4 Results on the IDC grading dataset

In this section, we have presented a systematic analysis of the Breast-NET framework's performance on the IDC grading dataset. The ROC curve of the Breast-NET model utilizing the IDC grading dataset is depicted in Fig. 8. We can see that the area under the curve for all three categories is more than 95% and not overlapping, indicating that the model is capable of distinguishing between three different grades. The accuracy and loss plots for IDC grading are shown in Fig. 9. The accuracy and loss plots demonstrate that the proposed model is well-suited for IDC grading tasks, as it achieves good performance on both the training and validation data, without suffering from overfitting or underfitting issues. The confusion matrix in Fig. 10 shows that the model achieved 94% classification accuracy and 0.0625 misclassification outcomes. We can also see that just three samples were misclassified as grade 2 when the real ground truth was grade 1. Table 7 shows the model's classification report; we can observe that the Breast-NET DCNN model produced promising outcomes such as accuracy 94%, precision 95%, recall 94%, and F1-score 94%. In addition, we conducted a detailed experiment with the existing transfer learning-based pre-trained DCNN models and compared our proposed model performance in terms of layers, disk space, number of model parameters, and testing accuracy; the comparison results are provided in Table 8. We can see that our proposed DCNN model outperformed the existing transfer learning-based pre-trained CNNs.

Furthermore, we have compared the performance of our proposed model to the state-of-the-art models available in the literatures, as shown in Table 9. Li et al. [42] achieved 93.01% classification accuracy using a pre-trained Xception CNN model as the backbone of their proposed multi task DCNN. The proposed framework has a significant rate of misclassification. Nanni et al. [19] presented a three-stage technique for breast cancer grading and achieved 93.7% testing accuracy, but the proposed approach necessitates human intervention. Yan et al. [20] and Yan et al. [43] proposed Nuclei aware CNN and NGNet for grading IDC and achieved 92.2% and 93.4% accuracy, respectively. However, in the preprocessing stage, they employed DeepLabV3+ with 11.85M model parameters to extract the nucleus patches from the histology data, so end-to-end training was not feasible and required a large computing cost. Lagree et al. [44] proposed a CAD system for rating IDC samples. Using the ensemble approach, they achieved 78.57% percent accuracy. We know that overfitting and underfitting are problems with ensemble learning, and end-to-end training is time-consuming and mainly computationally expensive. Secondly, the suggested model produces both false-positive and false-negative outcomes. Abdelli et al. [21] used pre-trained ResNet-50 &

Table 6 Comparison of the Breast-NET model with the state-of-the-art models on the BreakHis dataset for binary-class, and multi-class classification

Study by	# of classes	Models	Precision	Recall	F1-score	Accuracy (%)
Saini and Susan [16]	Malignant & Benign	VGGIN-Net	–	–	0.91 / 0.75	96.15
Vo et al. [4]	Malignant & Benign	Inception networks + gradient boosting trees classifier	–	–	–	95.5
Toğaçar et al. [26]	Malignant & Benign	Breast-Net	0.98	0.98	0.98	98.8
Garg et al. [17]	Malignant & Benign	MobilNetV2, InceptionV4, and ResNet-50	0.96	0.98	0.96	98.07
George et al. [28]	Malignant & Benign	AlexNet, ResNet-18, ResNet-50, ResNet-101, and GoogleNet + SVM	–	0.97	–	96.91
George et al. [29]	Malignant & Benign	NucDeep + FF + SVM	–	0.97	–	96.66
Rashmi et al. [18]	Malignant & Benign	BCHisto-Net CNN	0.90	0.89	0.89	89
Liu et al. [30]	Malignant & Benign	LBSE framework	0.94	0.85	0.89	86
Gupta and Bhavsar [31]	Malignant & Benign	Partially independent framework	–	–	–	94.66
Pratiher et al. [32]	Malignant & Benign	Manifold encoding + bidirectional LSTM	–	–	–	96.47
Kumar et al. [33]	Malignant & Benign	H& E stain + VGG-16 + SVM	–	–	0.97	97
Gour et al. [34]	Malignant & Benign	ResHist CNN	0.92	0.90	0.91	92.52
Wang et al. [35]	Malignant & Benign	FE-BkCapsNet	–	0.94	–	93.7
Abbasniya et al. [36]	Malignant & Benign	IRv2-CXL	–	–	0.97	96.46
Saini and Susan [37]	Malignant & Benign	DCGAN + VGG-16 CNN	–	–	0.94	94.75
Man et al. [38]	Malignant & Benign	DenseNet121-AnoGAN	0.92	0.95	0.94	91.77
Bardou et al. [40]	Malignant & Benign	CNN + KNN	–	–	–	84.49
Bardou et al. [40]	Malignant & Benign	CNN + RBF SVM	–	–	–	82.90
Bardou et al. [40]	Malignant & Benign	CNN + Linear SVM	–	–	–	86.60
Bardou et al. [40]	Malignant & Benign	CNN + Random Forest	–	–	–	84.08
Bardou et al. [40]	Malignant & Benign	CNN + Original data	–	–	–	94.25
Bardou et al. [40]	Malignant & Benign	CNN + Augmented data	0.97	0.97	0.97	96.52
Bardou et al. [40]	Malignant & Benign	CNN + SVM	–	–	–	92.82
Bardou et al. [40]	Malignant & Benign	CNN + Ensemble	–	–	–	97.36
Heikal et al. [55]	Malignant & Benign	Custom CNN	0.97	0.93	0.90	93.13
Rana et al. [56]	Malignant & Benign	Xception	0.76	0.87	0.85	83.09

Table 6 (continued)

Study by	# of classes	Models	Precision	Recall	F1-score	Accuracy (%)
Ijaz et al. [57]	Malignant & Benign	CBAM-VGGNet	–	0.95	0.98	97.66
Maleki et al. [58]	Malignant & Benign	DenseNet-201+XGBoost	0.91	0.96	0.94	91.9
Present work	Malignant & Benign	Breast-NET	**0.97**	**0.98**	**0.98**	**98.11**
Bardou et al. [40]	Multi-Class	CNN + KNN	–	–	–	68.73
Bardou et al. [40]	Multi-Class	CNN + RBF SVM	–	–	–	69.75
Bardou et al. [40]	Multi-Class	CNN + Linear SVM	–	–	–	67.85
Bardou et al. [40]	Multi-Class	CNN + Random Forest	–	–	–	67.31
Bardou et al. [40]	Multi-Class	CNN + Original data	–	–	–	82.47
Bardou et al. [40]	Multi-Class	CNN + Augmented data	0.82	0.82	0.82	82.53
Bardou et al. [40]	Multi-Class	CNN + SVM	–	–	–	80.30
Bardou et al. [40]	Multi-Class	CNN + Ensemble	–	–	–	85.04
Sharma and Mehra [39]	Multi-Class	AlexNet	0.86	0.84	0.84	85.83
Present work	Multi-Class	Breast-NET	**0.86**	**0.92**	**0.89**	**90.34**

Bold values to highlight our research findings and results in comparison with the state of-the-art findings

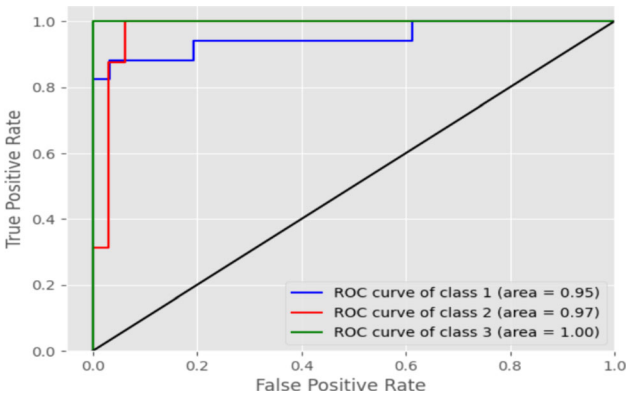

Fig. 8 The ROC curves of the Breast-NET model using the IDC grading dataset

MobileNet CNNs for grading breast cancer samples and achieved classification accuracy of 92.39% & 93.48%. Finally, the experimental findings in Table 9 reveal that the Breast-NET DCNN outperformed the state-of-the-art models.

4.5 Results on the IDC dataset

Here, we will discuss the experimental findings and analysis of the Breast-NET architecture on the IDC dataset. To demonstrate the superiority of the proposed model, we performed rigorous statistical performance assessment measures on the IDC dataset, as we did on the other two datasets. The ROC curve in Fig. 11 shows that the

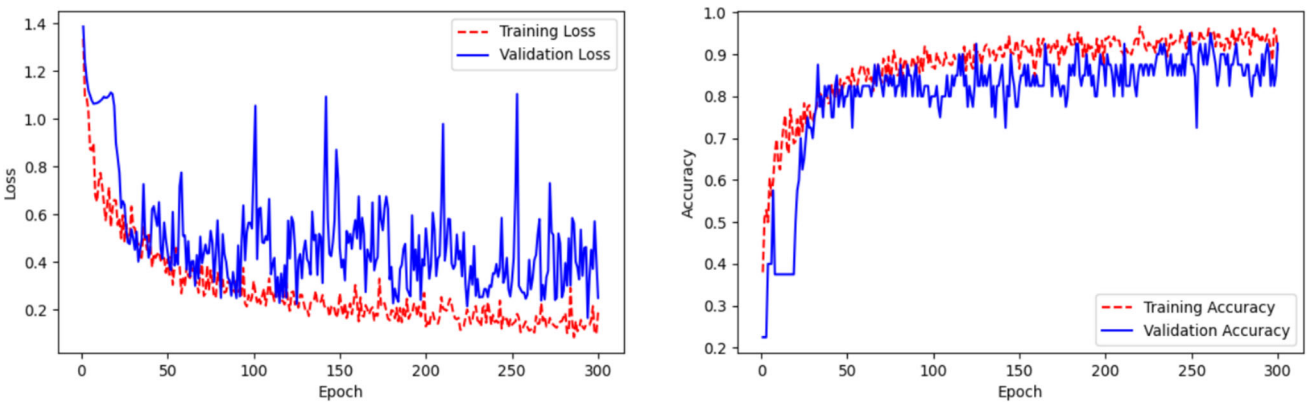

Fig. 9 The accuracy and loss plots of the Breast-NET model using the IDC grading dataset

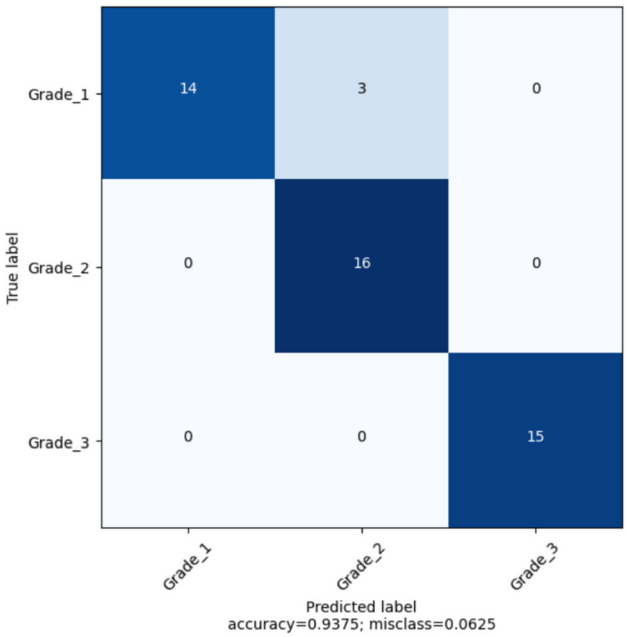

Fig. 10 The confusion matrix of the Breast-NET model using the IDC grading dataset

Table 7 Classification report of Breast-NET model on the IDC grading dataset

	Precision	Recall	F1-score
Class grade 1	1.00	0.82	0.90
Class grade 2	0.84	1.00	0.91
Class grade 3	1.00	1.00	1.00
Accuracy			94
Macro avg	0.95	0.94	0.94
Weighted avg	0.95	0.94	0.94

suggested model can differentiate between the IDC positive and IDC negative categories, as the area under the curve value for both classes is 96% and they do not overlap. The accuracy and loss plots for the IDC dataset are shown in Fig. 12. The accuracy and loss plots indicating the success of the proposed model for the IDC dataset without overfitting or underfitting are very promising. It demonstrates that the Breast-NET model has learned the relevant features from the histology images and can generalize well to new, unseen data. The confusion matrix in Fig. 13 illustrates the proposed model's overall classification performance on the IDC dataset. In the confusion matrix, levels 0 and 1 reflect the IDC negative and positive categories, respectively. Table 10 shows the classification report; we can see that the model achieved overall 90.44% accuracy, 89% precision, 87% recall, and 88% F1-score for classification of IDC positive and negative categories. In addition, we conducted detailed experimental research with transfer learning-based pre-trained CNNs using the IDC dataset and evaluated their performance; the findings are displayed in Table 11. Table 11 shows that the proposed model outperforms the pre-trained CNNs.

Furthermore, we have compared the proposed approach's performance against the state-of-the-art methodologies listed in Table 12. Cruz-Roa et al. [22] suggested a three-layered CNN for IDC positive and negative histopathology sample classification. The proposed method achieved 84.23% accuracy, 71% F1-score, 65% precision, and 79% recall. Liu et al. [5] used a pre-trained AlexNet CNN model to classify invasive ductal carcinoma and achieved 86.31% accuracy. Celik et al. [23] utilized pre-trained ResNet-50 for IDC negative and positive category detection. The proposed approach achieved 90.96% test accuracy; however, the computational complexity of the proposed model is 4.12G, which is 29 times greater than ours. Similarly, Wang et al. [45] and Romero et al. [46] employed CNN-GRU and Inception CNN for IDC(+) and IDC(−) sample classification and achieved test accuracy of 86.21% and 89%, respectively. Reza and Ma [24] presented a six-layer CNN model for IDC classification and achieved 85.48% accuracy. Janowczyk and Madabhushi [47] used the AlexNet CNN model, as did Liu et al. [5],

Table 8 Comparison of the Breast-NET model performance with other popular transfer learning-based pre-trained DCNN models on the IDC grading dataset

DCNNs	Input dimension	Layers	Size (Mb)	#Params(M)	FLOPs	Accuracy (%)
MobileNetV2 [49]	224 × 224 × 3	157	23.4	2.2	0.30G	78
VGG-19 [50]	224 × 224 × 3	24	166	20	19.6G	60
ResNet-50 [51]	224 × 224 × 3	178	124	23.5	3.88G	65
VGG-16 [50]	224 × 224 × 3	21	155	14.7	15.5G	56
MobileNetV1 [52]	224 × 224 × 3	89	37.1	3.2	0.57G	65
Inception-v3 [53]	299 × 299 × 3	314	192	21.8	5.73G	93.5
DenseNet-201 [54]	224 × 224 × 3	709	124	18.3	4.32G	94
Breast-NET	256 × 256 × 3	52	1.87	0.135	0.141G	94

Table 9 Comparison of the Breast-NET model with the state-of-the-art models on the IDC grading dataset

Study by	# of classes	Models	Precision	Recall	F1-score	Accuracy (%)
Li et al. [42]	Grade 1 & Grade 2 & Grade 3	Xception	–	–	–	93.01
Nanni et al. [19]	Grade 1 & Grade 2 & Grade 3	ReNet50 + SVM classifier	–	–	–	93.7
Yan et al. [43]	Grade 1 & Grade 2 & Grade 3	NGNet	–	0.95	–	93.4
Yan et al. [20]	Grade 1 & Grade 2 & Grade 3	Nuclei aware CNN	–	–	–	92.2
Lagree et al. [44]	Grade 1 & Grade 2 & Grade 3	CAD system	–	0.83	0.82	78.57
Abdelli et al. [21]	Grade 1 & Grade 2 & Grade 3	ResNet-50 & MobileNet	0.92 & 0.93	0.92 & 0.93	0.92 & 0.93	92.39 & 93.48
Present work	Grade 1 & Grade 2 & Grade 3	Breast-NET	**0.95**	**0.94**	**0.94**	**94**

Bold values to highlight our research findings and results in comparison with the state of-the-art findings

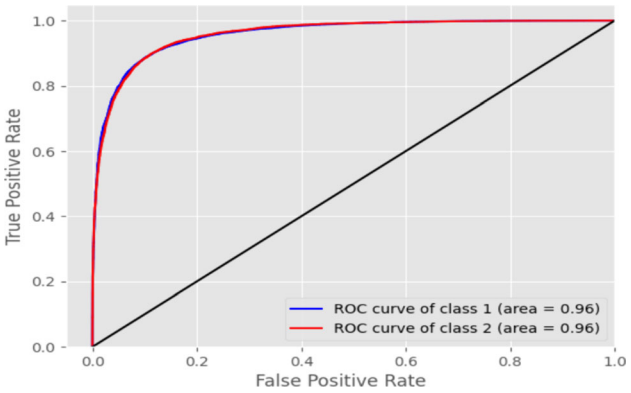

Fig. 11 The ROC curves of the Breast-NET model using the IDC dataset

and achieved 84.68% testing accuracy. Abdolahi et al. [48] developed a four-layer CNN for classifying IDC(+) and IDC(-). The proposed model scored 85.62% test accuracy, 86% precision, and an F1-score of 83%. Finally, we can see that our suggested DCNN model outperforms the state-of-the-art techniques.

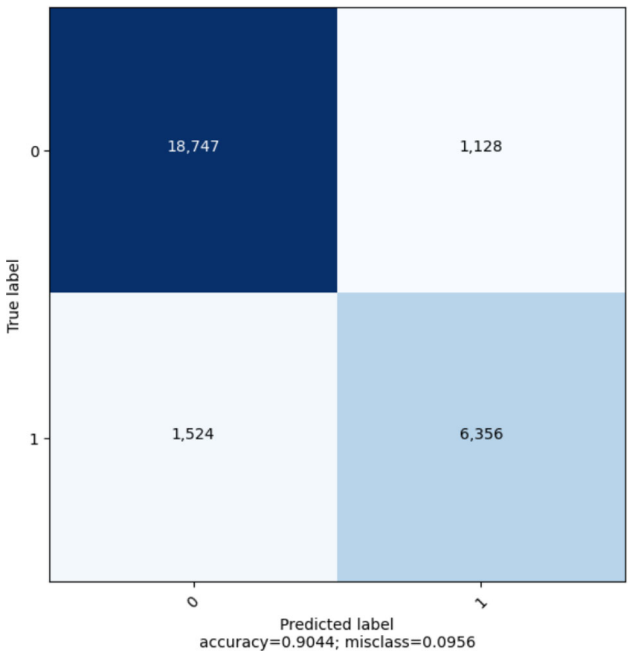

Fig. 13 The confusion matrix of the Breast-NET model using the IDC dataset

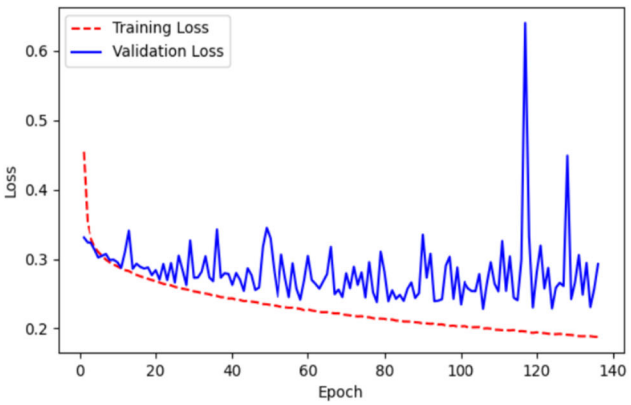

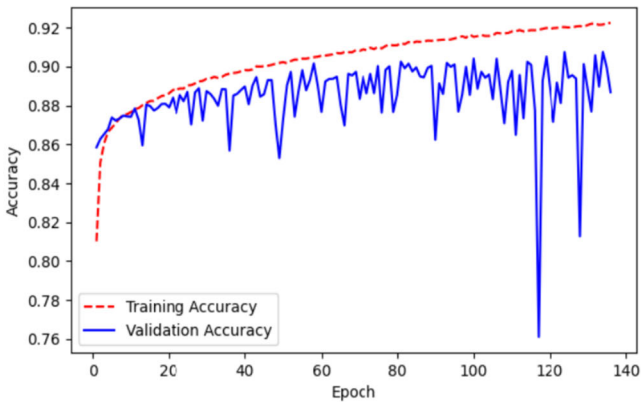

Fig. 12 The loss and accuracy of the Breast-NET model using the IDC dataset

Table 10 Classification report of Breast-NET model on the IDC dataset

	Precision	Recall	F1-score
Class IDC(−)	0.92	0.94	0.93
Class IDC(+)	0.85	0.81	0.83
Accuracy			90.44
Macro avg	0.89	0.87	0.88
Weighted avg	0.90	0.90	0.90

Table 11 Comparison of the Breast-NET model performance with other transfer learning-based pre-trained DCNN models on the IDC dataset

DCNNs	Input dimension	Layers	Size (Mb)	# Params (M)	FLOPs	Accuracy (%)
MobileNetV2 [49]	$50 \times 50 \times 3$	157	23.4	2.2	0.30G	72
VGG-19 [50]	$50 \times 50 \times 3$	24	166	20	19.6G	87
ResNet-50 [51]	$50 \times 50 \times 3$	178	124	23.5	3.88G	83
VGG-16 [50]	$50 \times 50 \times 3$	21	155	14.7	15.5G	88
MobileNetV1 [52]	$50 \times 50 \times 3$	89	37.1	3.2	0.57G	90
Inception-v3 [53]	$75 \times 75 \times 3$	314	168	21.8	5.73G	87
DenseNet-201 [54]	$50 \times 50 \times 3$	709	124	18.3	4.32G	87
Breast-NET	$50 \times 50 \times 3$	52	1.86	0.135	0.006G	90.44

Table 12 Comparison of the Breast-NET model with the state-of-the-art models on the IDC dataset

Study by	# of Classes	Models	Precision	Recall	F1-score	Accuracy (%)
Cruz-Roa et al. [22]	IDC(+) & IDC(−)	Three-layered CNN	0.65	0.79	0.71	84.23
Liu et al. [5]	IDC(+) & IDC(−)	AlexNet	–	–	–	86.31
Celik et al. [23]	IDC(+) & IDC(−)	ResNet-50	0.94	0.93	0.94	90.96
Wang et al. [45]	IDC(+) & IDC(−)	CNN-GRU	0.85	0.85	0.88	86.21
Romero et al. [46]	IDC(+) & IDC(−)	Inception CNN	–	–	0.89	89
Reza and Ma [24]	IDC(+) & IDC(−)	Six-layer CNN	–	0.80	0.84	85.48
Janowczyk and Madabhushi [47]	IDC(+) & IDC(−)	AlexNet	–	–	0.76	84.68
Abdolahi et al. [48]	IDC(+) & IDC(−)	Four layer CNN	0.86	–	0.83	85.62
Present work	IDC(+) & IDC(−)	Breast-NET	**0.89**	**0.87**	**0.88**	**90.44**

Bold values to highlight our research findings and results in comparison with the state of-the-art findings

5 Conclusion and future work

In this study, we have presented a novel lightweight deep learning framework called Breast-NET for detecting and grading breast cancer using histological images. The performance of our proposed model was evaluated on three different breast histological image datasets, each with distinct hallmark signature characteristics. To enhance generalization and reduce space and computational complexity, Breast-NET incorporates a combination of channel attention modules, multilevel feature extraction, separable convolution layers, and global average pooling layers.

We conducted a comprehensive ablation study, assessing various factors such as the number of Breast-NET blocks, attention modules, training with or without early stopping, minority class weight, and number of layers, to demonstrate the design considerations of our model. The experimental results revealed that Breast-NET achieved impressive test accuracies of 98.11% and 90.34% for binary and multi-class classification on the BreaKHis dataset, with only 52 layers, a size of 1.86Mb, and 0.141G FLOPs. For IDC grading and IDC datasets, our model achieved 94% and 90.44% test accuracy, respectively. Moreover, the

false-positive and false-negative rates were minimal, and the testing time complexity was only 0.19s per image.

Compared with transfer learning-based approaches, we observed that although they are effective for breast cancer detection, they suffer from high misclassification rates, computational expenses, and additional disk space requirements. In contrast, our Breast-NET model outperformed state-of-the-art research and is particularly suitable for FPGA implementations due to its low space, time, and computational complexity.

As part of our future work, we aim to enhance the generalization ability of Breast-NET by exploring new architectural design considerations and deploying them on FPGA devices. Additionally, we plan to investigate the efficiency of deep learning for detecting and grading cancers in other parts of the body, further expanding the scope and impact of our research.

Author contributions All authors contributed equally.

Funding The authors declare that no funds, grants, or other support were received during the preparation of this manuscript.

Data availability The data that support the finding of this study are available from [22, 25, 41].

Declarations

Conflict of interest The authors have no relevant financial or nonfinancial interests to disclose.

Ethical approval This article does not contain any studies with human or animal subjects performed by any of the authors. This study exclusively utilized publicly available data, which have been appropriately cited.

Consent to participate This study did not involve the participation of human subjects.

Consent to publish This study did not involve the participation of human subjects.

References

1. Sung H, Ferlay J, Siegel RL, Laversanne M, Soerjomataram I, Jemal A, Bray F (2021) Global cancer statistics 2020: Globocan estimates of incidence and mortality worldwide for 36 cancers in 185 countries. CA: Cancer J Clin 71(3):209–249
2. Breast cancer awareness month: Stay vigilant, stay healthy. https://www.thehindu.com/life-and-style/october-marks-breast-cancer-awareness-month-heres-what-we-need-to-know-and-do-to-keep-the-disease-away/article66030432.ece. Accessed: 2023-07-26
3. Joy JE, Penhoet EE, Petitti DB, *et al.* (2005) Saving Women's Lives: Strategies for Improving Breast Cancer Detection and Diagnosis. national academies press Washington, DC
4. Vo DM, Nguyen N-Q, Lee S-W (2019) Classification of breast cancer histology images using incremental boosting convolution networks. Inf Sci 482:123–138
5. Liu M, Hu L, Tang Y, Wang C, He Y, Zeng C, Lin K, He Z, Huo W (2022) A deep learning method for breast cancer classification in the pathology images. IEEE J Biomed Health Inform 26(10):5025–5032
6. Chakraborty M, Dhavale SV, Ingole J (2021) Corona-nidaan: lightweight deep convolutional neural network for chest x-ray based covid-19 infection detection. Appl Intell 51(5):3026–3043
7. Chakraborty M, Dhavale SV, Ingole J (2022) Two-stage deep learning architecture for chest x-ray-based covid-19 prediction. In: Advances in Deep Learning for Medical Image Analysis, pp. 19–37. CRC Press
8. Hasan MM, Chakraborty M, Raj AAB (2023) A hyper-parameters-tuned r-pca+ svm technique for suav targets classification using the range-/micro-doppler signatures. IEEE Trans Radar Syst
9. Chakraborty M, Kumawat HC, Dhavale SV et al (2022) Diat-radharnet: a lightweight dcnn for radar based classification of human suspicious activities. IEEE Trans Instrum Meas 71:1–10
10. Kumawat HC, Chakraborty M, Raj AAB (2022) Diat-radsatnet-novel lightweight dcnn architecture for micro-doppler-based small unmanned aerial vehicle (suav) targets' detection and classification. IEEE Trans Instrum Meas 71:1–11
11. Kumawat HC, Chakraborty M, Raj AAB, Dhavale SV (2021) Diat-μsat: Small aerial targets' micro-doppler signatures and their classification using cnn. IEEE Geosci Remote Sens Lett 19:1–5
12. Chakraborty M, Kumawat HC, Dhavale SV, Raj AAB (2022) Diat-μ radhar (micro-doppler signature dataset) & μ radnet (lightweight dcnn)-for human suspicious activity recognition. IEEE Sens J 22(7):6851–6858
13. Chakraborty M, Kumawat HC, Dhavale SV et al (2022) Application of dnn for radar micro-doppler signature-based human suspicious activity recognition. Pattern Recogn Lett 162:1–6
14. Chakraborty M, Pramanick A, Vikrant Dhavale S (2020) Two-stream mid-level fusion network for human activity detection. In: International Conference on Innovative Computing and Communications: Proceedings of ICICC 2020, Volume 2, pp. 331–343. Springer
15. Chakraborty M, Pramanick A, Dhavale SV (2020) Mobisamadhaan-intelligent vision-based smart city solution. In: International Conference on Innovative Computing and Communications: Proceedings of ICICC 2020, Volume 1, pp. 329–345. Springer
16. Saini M, Susan S (2022) Vggin-net: deep transfer network for imbalanced breast cancer dataset. IEEE/ACM Trans Comput Biol Bioinf
17. Garg S, Singh P (2022) Transfer learning based lightweight ensemble model for imbalanced breast cancer classification. IEEE/ACM Trans Comput Biol Bioinf
18. Rashmi R, Prasad K, Udupa CBK (2021) Bchisto-net: Breast histopathological image classification by global and local feature aggregation. Artif Intell Med 121:102191
19. Nanni L, Ghidoni S, Brahnam S (2021) Deep features for training support vector machines. J Imag 7(9):177
20. Yan R, Li J, Rao X, Lv Z, Zheng C, Dou J, Wang X, Ren F, Zhang F (2020) Nanet: nuclei-aware network for grading of breast cancer in he stained pathological images. In: 2020 IEEE International Conference on Bioinformatics and Biomedicine (BIBM), pp. 865–870. IEEE
21. Abdelli A, Saouli R, Djemal K, Youkana I (2020) Combined datasets for breast cancer grading based on multi-cnn architectures. In: 2020 Tenth International Conference on Image Processing Theory, Tools and Applications (IPTA), pp. 1–7. IEEE
22. Cruz-Roa A, Basavanhally A, Gonzàlez F, Gilmore H, Feldman M, Ganesan S, Shih N, Tomaszewski J, Madabhushi A (2014)

Automatic detection of invasive ductal carcinoma in whole slide images with convolutional neural networks. In: Medical Imaging 2014: Digital Pathology, vol. 9041, p. 904103. SPIE
23. Celik Y, Talo M, Yildirim O, Karabatak M, Acharya UR (2020) Automated invasive ductal carcinoma detection based using deep transfer learning with whole-slide images. Pattern Recogn Lett 133:232–239
24. Reza MS, Ma J (2018) Imbalanced histopathological breast cancer image classification with convolutional neural network. In: 2018 14th IEEE International Conference on Signal Processing (ICSP), pp. 619–624. IEEE
25. Spanhol FA, Oliveira LS, Petitjean C, Heutte L (2015) A dataset for breast cancer histopathological image classification. IEEE Trans Biomed Eng 63(7):1455–1462
26. Toğçar M, Özkurt KB, Ergen B, Cömert Z (2020) Breastnet: A novel convolutional neural network model through histopathological images for the diagnosis of breast cancer. Physica A 545:123592
27. Aresta G, Araújo T, Kwok S, Chennamsetty SS, Safwan M, Alex V, Marami B, Prastawa M, Chan M, Donovan M et al (2019) Bach: Grand challenge on breast cancer histology images. Med Image Anal 56:122–139
28. George K, Faziludeen S, Sankaran P et al (2020) Breast cancer detection from biopsy images using nucleus guided transfer learning and belief based fusion. Comput Biol Med 124:103954
29. George K, Sankaran P et al (2020) Computer assisted recognition of breast cancer in biopsy images via fusion of nucleus-guided deep convolutional features. Comput Methods Programs Biomed 194:105531
30. Liu X, Kang X, Nie X, Guo J, Wang S, Yin Y (2022) Learning binary semantic embedding for large-scale breast histology image analysis. IEEE J Biomed Health Inform 26(7):3240–3250
31. Gupta V, Bhavsar A (2019) Partially-independent framework for breast cancer histopathological image classification. In: Proceedings of the IEEE/CVF Conference on Computer Vision and Pattern Recognition Workshops, pp. 0–0
32. Pratiher S, Chattoraj S, Agarwal S, Bhattacharya S (2018) Grading tumor malignancy via deep bidirectional lstm on graph manifold encoded histopathological image. In: 2018 IEEE International Conference on Data Mining Workshops (ICDMW), pp. 674–681. IEEE
33. Kumar A, Singh SK, Saxena S, Lakshmanan K, Sangaiah AK, Chauhan H, Shrivastava S, Singh RK (2020) Deep feature learning for histopathological image classification of canine mammary tumors and human breast cancer. Inf Sci 508:405–421
34. Gour M, Jain S, Sunil Kumar T (2020) Residual learning based cnn for breast cancer histopathological image classification. Int J Imaging Syst Technol 30(3):621–635
35. Wang P, Wang J, Li Y, Li P, Li L, Jiang M (2021) Automatic classification of breast cancer histopathological images based on deep feature fusion and enhanced routing. Biomed Signal Process Control 65:102341
36. Abbasniya MR, Sheikholeslamzadeh SA, Nasiri H, Emami S (2022) Classification of breast tumors based on histopathology images using deep features and ensemble of gradient boosting methods. Comput Electr Eng 103:108382
37. Saini M, Susan S (2020) Deep transfer with minority data augmentation for imbalanced breast cancer dataset. Appl Soft Comput 97:106759
38. Man R, Yang P, Xu B (2020) Classification of breast cancer histopathological images using discriminative patches screened by generative adversarial networks. IEEE Access 8:155362–155377
39. Sharma S, Mehra R (2020) Effect of layer-wise fine-tuning in magnification-dependent classification of breast cancer histopathological image. Vis Comput 36(9):1755–1769
40. Bardou D, Zhang K, Ahmad SM (2018) Classification of breast cancer based on histology images using convolutional neural networks. IEEE Access 6:24680–24693
41. Dimitropoulos K, Barmpoutis P, Zioga C, Kamas A, Patsiaoura K, Grammalidis N (2017) Grading of invasive breast carcinoma through grassmannian vlad encoding. PLoS ONE 12(9):0185110
42. Li L, Pan X, Yang H, Liu Z, He Y, Li Z, Fan Y, Cao Z, Zhang L (2020) Multi-task deep learning for fine-grained classification and grading in breast cancer histopathological images. Multimedia Tools Appl 79:14509–14528
43. Yan R, Ren F, Li J, Rao X, Lv Z, Zheng C, Zhang F (2022) Nuclei-guided network for breast cancer grading in he-stained pathological images. Sensors 22(11):4061
44. Lagree A, Shiner A, Alera MA, Fleshner L, Law E, Law B, Lu F-I, Dodington D, Gandhi S, Slodkowska EA et al (2021) Assessment of digital pathology imaging biomarkers associated with breast cancer histologic grade. Curr Oncol 28(6):4298–4316
45. Wang X, Ahmad I, Javeed D, Zaidi SA, Alotaibi FM, Ghoneim ME, Daradkeh YI, Asghar J, Eldin ET (2022) Intelligent hybrid deep learning model for breast cancer detection. Electronics 11(17):2767
46. Romero FP, Tang A, Kadoury S (2019) Multi-level batch normalization in deep networks for invasive ductal carcinoma cell discrimination in histopathology images. In: 2019 IEEE 16th International Symposium on Biomedical Imaging (ISBI 2019), pp. 1092–1095. IEEE
47. Janowczyk A, Madabhushi A (2016) Deep learning for digital pathology image analysis: a comprehensive tutorial with selected use cases. J Pathol Inf 7(1):29
48. Abdolahi M, Salehi M, Shokatian I, Reiazi R (2020) Artificial intelligence in automatic classification of invasive ductal carcinoma breast cancer in digital pathology images. Med J Islam Repub Iran 34:140
49. Sandler M, Howard A, Zhu M, Zhmoginov A, Chen L-C (2018) Mobilenetv2: Inverted residuals and linear bottlenecks. In: Proceedings of the IEEE Conference on Computer Vision and Pattern Recognition, pp. 4510–4520
50. Simonyan K, Zisserman A (2014) Very deep convolutional networks for large-scale image recognition. arXiv preprint arXiv:1409.1556
51. He K, Zhang X, Ren S, Sun J (2016) Deep residual learning for image recognition. In: Proceedings of the IEEE Conference on Computer Vision and Pattern Recognition, pp. 770–778
52. Howard AG, Zhu M, Chen B, Kalenichenko D, Wang W, Weyand T, Andreetto M, Adam H (2017) Mobilenets: Efficient convolutional neural networks for mobile vision applications. arXiv preprint arXiv:1704.04861
53. Szegedy C, Vanhoucke V, Ioffe S, Shlens J, Wojna Z (2016) Rethinking the inception architecture for computer vision. In: Proceedings of the IEEE Conference on Computer Vision and Pattern Recognition, pp. 2818–2826
54. Huang G, Liu Z, Van Der Maaten L, Weinberger KQ (2017) Densely connected convolutional networks. In: Proceedings of the IEEE Conference on Computer Vision and Pattern Recognition, pp. 4700–4708
55. Heikal A, El-Ghamry A, Elmougy S, Rashad M (2024) Fine tuning deep learning models for breast tumor classification. Sci Rep 14(1):10753
56. Rana M, Bhushan M (2023) Classifying breast cancer using transfer learning models based on histopathological images. Neural Comput Appl 35(19):14243–14257
57. Ijaz A, Raza B, Kiran I, Waheed A, Raza A, Shah H, Aftan S (2023) Modality specific cbam-vggnet model for the classification of breast histopathology images via transfer learning. IEEE Access 11:15750–15762

58. Maleki A, Raahemi M, Nasiri H (2023) Breast cancer diagnosis from histopathology images using deep neural network and xgboost. Biomed Signal Process Control 86:105152